Shock compression of monocrystalline copper: Experiments, characterization, and analysis

Buyang Cao [a,*], David H. Lassila [b], Chongxiang Huang [c], Yongbo Xu [c], Marc André Meyers [d]

[a] Department of Mechanical Engineering, The Johns Hopkins University, Baltimore, MD 21218, United States
[b] Lawrence Livermore National Laboratory, Livermore, CA 94550, United States
[c] Shenyang National Laboratory for Materials Science, Institute of Metal Research, Chinese Academy of Sciences, Shenyang 110016, China
[d] Departments of Mechanical and Aerospace Engineering and Nanoengineering, UC San Diego, La Jolla, San Diego, CA 92093, United States

ARTICLE INFO

ABSTRACT

Monocrystalline copper samples with [0 0 1] and [2 2 1] orientations were subjected to shock/recovery experiments at 30 and 57 GPa and 90 K. The slip system activity and the microstructural evolution were investigated. Different defect structures, including dislocations, stacking faults, twins, microbands, and recrystallized grains were observed in the specimens. The residual microstructures were dependent on crystalline orientation and pressure. The differences with crystalline orientations are most likely due to different resolved shear stresses on specific crystalline planes. The geometric relationships between the shock propagation direction and crystalline orientation are presented under uniaxial strain. It is shown that the [2 2 1] orientation, by virtue of having fewer highly activated slip systems, exhibits greater concentration of deformation with more intense shear on the primary system. This, in turn leads to greater local temperature rise and full recrystallization, in spite of the thermodynamic residual temperature of ~500 K and rapid cooling (within 20 s) to ambient temperature. The profuse observation of microbands is interpreted in terms of the mechanism proposed by Huang and Gray [J.C. Huang, G.T. Gray III, Acta Metallurgica 37 (1989) 3335–3347].

© 2009 Elsevier B.V. All rights reserved.

1. Introduction

The effect of shock compression on the microstructure and mechanical properties of copper has been extensively investigated. The diversity of the post-shock microstructures has been an intriguing topic of research for a long period of time. Shock/recovery experiments have provided an effective means to study the dynamic behavior of materials. Gray [1], Murr and co-workers [2,3], and Grace [4] observed different substructures on post-shocked copper: cell structures, sub-grains and deformation twins. Gray et al. [5] was the first to point out that the dislocation structure depended on the residual (post-shock) strain; the tendency for banding increased with increasing residual strain. The first researchers to identify and explain the slip-twinning transition in shock compression were Johari and Thomas [6] and Nolder and Thomas [7,8]. De Angelis and Cohen [9] found a threshold twinning stress that is dependent on shock propagation direction. The quasistatic and dynamic deformation behavior of shocked copper has also been widely investigated [10–13]. Follansbee and Gray [14] measured the yield stress and strain hardening behavior at

strain-rates ranging from 10^{-3} to $10^4 \, \mathrm{s}^{-1}$, and Kocks and Follansbee [14–17] modeled the high-strain-rate results. Andrade et al. and Meyers et al. [18–20] investigated the deformation of shocked copper at high-strains and high-strain-rates; the microstructure evolution, dynamic recrystallization and the effect of grain size were studied.

The mechanical behavior of shocked copper has also been investigated by Gourdin and Lassila [21]. More recently, Lassila et al. [22] studied the shock compression response of polycrystalline copper at low temperature by cooling the assembly with liquid nitrogen. This was done with the objective of maximizing the pressure range and minimizing post-shock recovery/recrystallization effects. The results presented in this paper extend the previous study of plate impacted polycrystalline copper at low temperature to monocrystals, with both symmetric [0 0 1] and asymmetric [2 2 1] crystal orientations. Fig. 1(a) is the standard stereographic projection, showing the corresponding positions of [0 0 1] and [$\bar{1}$ 2 2]. These two orientations were chosen because of the differences in respond they solicit. [0 0 1] has eight slip systems with the same Schmid factor, whereas [$\bar{1}$ 2 2] is on the great circle between [1 1 1] and [0 1 1]. It has only one slip system with the highest Schmid factor.

The formation of microbands, with thickness of approximately 0.2 μm, was first observed in shock compression by Gray [23] and Huang and Gray [24,25]. Huang and Gray [24] proposed a mecha-

* Corresponding author. Fax: +1 10 410 516 4316.
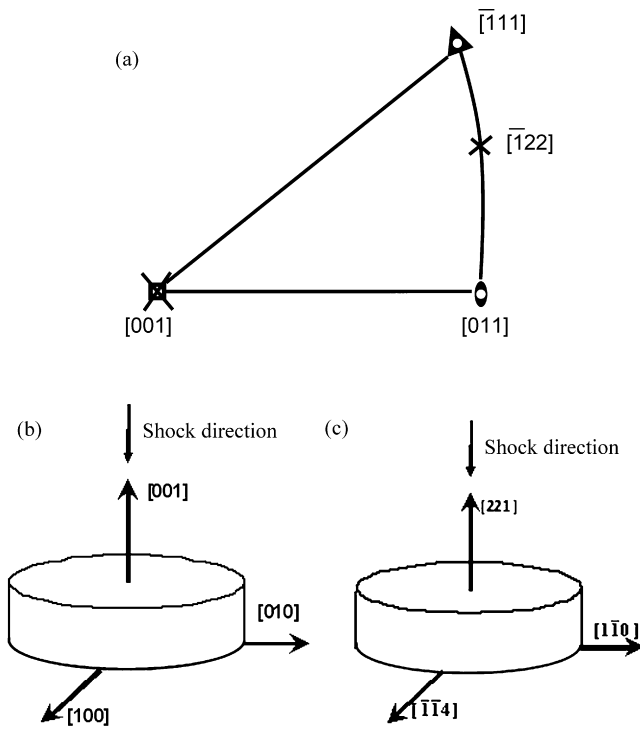 *E-mail addresses:* bcao3@jhu.edu, caobuyang@yahoo.com (B. Cao).

Fig. 1. (a) Standard stereographic projection, which shows the corresponding positions of [0 0 1] and [$\bar{1}$22]; (b) geometry of the three perpendicular crystalline orientations for [0 0 1] monocrystal; (c) geometry of the three perpendicular crystalline orientations for [2 2 1] monocrystal.

Fig. 2. SEM-ECC of back surface for 30 GPa [0 0 1] samples: (a) slip band traces; (d) two traces of slip bands with 90° apart.

nism for the formation of these microbands based on the formation of double dislocation walls forming on the primary slip plane followed by the activation of secondary slip leading to reactions and the formation of Cottrell–Lomer locks. Sanchez et al. [26] confirmed the presence of these microbands in the shock loading of copper and reported that the propensity for band formation increased with increasing grain size. They present a similar interpretation for their formation, based on double dislocation walls. Wagner et al. [27] observed similar microbands in conventionally deformed copper as did many other researchers.

2. Experimental techniques

Monocrystalline copper samples, with two orientations [0 0 1] and [2 2 1], were shock compressed at 30 and 57 GPa in shock/recovery experiments at the low temperature of 90 K. The setup used for this experiment was described in a previous paper [22]. The copper samples, with a diameter of 20 mm and thickness of 4.5 mm, were shocked by an explosion-driven flyer plate, providing initial pulse duration of 1.4 μs for 30 GPa and 1.1 μs for 57 GPa.

Scanning electron microscopy (Electron Channeling Contrast [28]) (SEM-ECC) and transmission electron microscopy (TEM) were performed after the shock/recovery experiments. Copper cylinders with 3 mm diameter and 4 mm length were prepared for SEM-ECC by mechanically polishing with sandpaper, and electro-etching in a solution of 1000 ml H_2O, 500 ml H_3PO_4, 500 ml C_2H_5OH, 10 g NH_2CONH_2, 100 ml $CH_3CH(OH)CH_3$. The SEM-ECC was conducted in a Cambridge S-360 Scanning Electron Microscope. This method of characterization reveals deformation markings and grains in a clear fashion. Samples for TEM were obtained by electro-polishing method. We were not only interested in the microstructure evolution along the shock propagation directions ([0 0 1] and [2 2 1]), but also in the defect structures perpendicular to the shock propagation
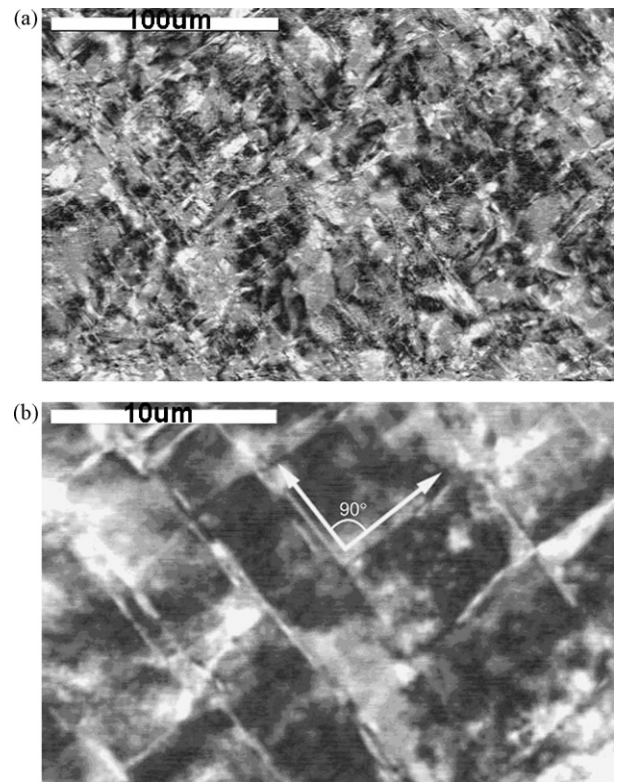
direction. Therefore, TEM was also used to explore the microstructure at a crystal orientation perpendicular to the shock propagation direction, i.e., [1 0 0] orientation in the [0 0 1] copper, and [1 1 0] in the [2 2 1] copper. The shapes of the TEM samples and their orientations with respect to the shock direction are illustrated in Fig. 1(b) and (c). The TEM work involved in this research was conducted on two instruments: a JEM 2000FX II with an operating voltage of 200 kV at the Shenyang National Laboratory for Materials Science, China, and a JEM 3010 with an operating voltage of 300 kV at the National Center for Electron Microscopy, Berkeley.

3. Microstructural analysis

3.1. [0 0 1] copper impacted at 30 GPa

Fig. 2 shows the SEM-ECC pictures from the 30 GPa post-shocked [0 0 1] specimen. Fig. 2(a) reveals that the back surface of the sample was full of slip band traces. Fig. 2(b) provides a more detailed view of the area with slip band traces. The presence of two sets of lines, which are spaced almost exactly 90° apart, is clear evidence for {1 1 1} traces on the plane of observation, (0 0 1).

The microstructure shown by TEM for the same specimen confirms that the deformation markings are slip bands and stacking faults [29]. Fig. 3(a) shows traces of the stacking faults. The thin foil has straight "boundaries" caused by fracturing along the slip bands, which was also found by SEM (as in Fig. 4). Fig. 3(b) shows the two sets of stacking faults as [$\bar{2}$ 2 0] and [2 2 0] traces in the (0 0 1) plane when the TEM electron beam direction is B = [0 0 1]. It seems that the stacking faults in [$\bar{2}$ 2 0] direction were formed before the [2 2 0] ones, because they are continuous, while the [2 2 0] stacking faults are segmented. The occurrence of stacking faults is comparable to that found by Meyers and co-workers [30] on laser-induced shock compression of monocrystalline copper.
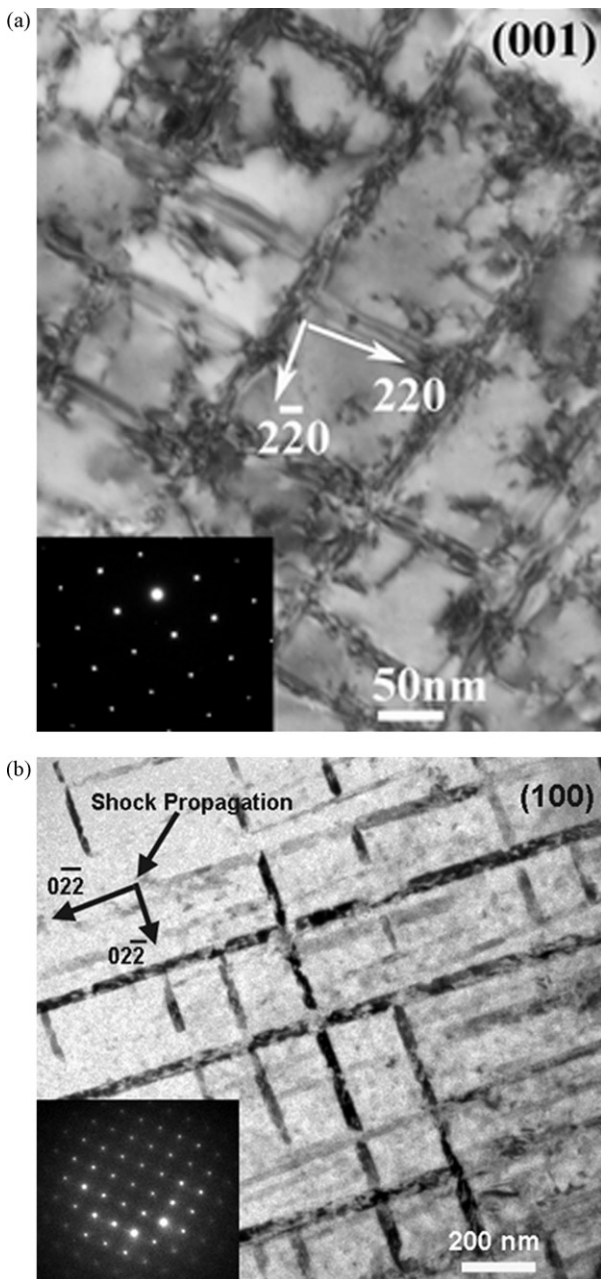
Fig. 3. (a) Two sets of perpendicular traces of the stacking faults shown on the (001) plane when the TEM electron beam direction is B = [0 0 1]; (b) TEM showing stacking faults on (100) plane in [0 0 1] shocked monocrystalline copper.

Very little work has been done using TEM to provide the three-dimensional picture of microstructural evolution during plate impact. Fig. 3(c) reveals the microstructure along the [1 0 0] crystal orientation shocked to 30 GPa. The [1 0 0] crystal orientation is perpendicular to the [0 0 1] shock direction ((0 0 1) shock front plane). Stacking faults similar to the ones on the (0 0 1) plane were observed on the (1 0 0) plane (Fig. 3(a) and (b)), which may indicate the stacking faults are distributed throughout the sample for the 30 GPa case. The traces of these stacking faults packets form an angle of 90°, which is exactly the expected angle.

3.2. [2 2 1] copper impacted at 30 GPa

Fig. 4 shows the SEM-ECC pictures for the [2 2 1] orientation. In Fig. 4(a) one trace is clear and the other is indicated by a dashed
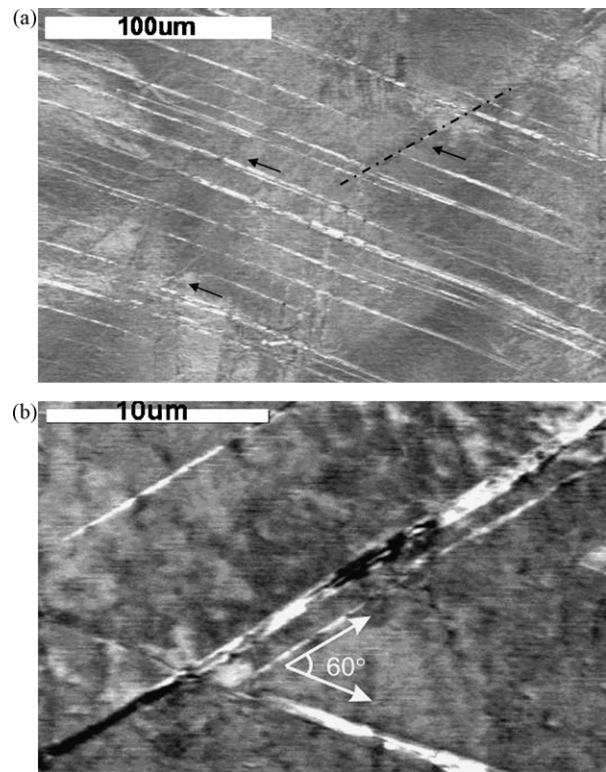

Fig. 4. SEM-ECC for 30 GPa [2 2 1] samples: (a) front surface of the sample along the shock propagation direction; (b) two microbands with 56° apart on the back surface.

line. Fig. 4(b), at a higher magnification, shows the details more clearly. Two traces of slip bands are present with an angle of 56°. As analyzed in Section 4.2 (Figs. 11 and 12), they are the traces of {1 1 1} planes on (2 2 1).

Although the substructure of the [2 2 1] copper shocked at 30 GPa is full of bands, the morphology of these bands varies throughout the sample. The formation of similar bands in shocked has been described by Gray and co-worker [24,25]. Microbands having widths of 20–30 nm were found within the larger bands. Fig. 5(a) shows the regular slip band morphology.

The microstructure on the (1 $\bar{1}$ 0) plane in the 30 GPa impacted [2 2 1] sample is shown in Fig. 5(b). Similar bands as shown in Fig. 5(a) were also observed. These bands align with [$\bar{1}$ 1 2] orientation, which indicates that they might be the traces of (1 $\bar{1}$ 1) plane on (1 1 0). The basic difference with the [0 0 1] crystal is that two (or more) systems are simultaneously activated in the former, whereas Fig. 5(a) and (b) shows primarily one trace.

In contrast with [0 0 1], one slip system is highly activated with minor activity in the cross-slip system. This is in full agreement with the calculations that will be presented in Section 4.

3.3. [0 0 1] copper impacted at 57 GPa

SEM-ECC shows the shock-induced structures of the surface perpendicular to the shock propagation direction (Fig. 6) consists of a mix of recrystallized grains (area **A** in the picture), and bands (area **B**) with a width of 15∼16 μm.

TEM confirms that the structure is not uniform. Microtwins, dislocation tangles, deformation bands, and slip bands are seen in the regions. The diversity of the post-shocked microstructures was induced by the high shock pressure and post-shock heating. Microtwins were observed throughout the sample (Fig. 7(a)). They have a ($\bar{1}$ $\bar{1}$ 1) habit plane at the electron beam direction of [0 1 1]. The sizes of these microtwins vary from 80 to 180 nm. Murr and
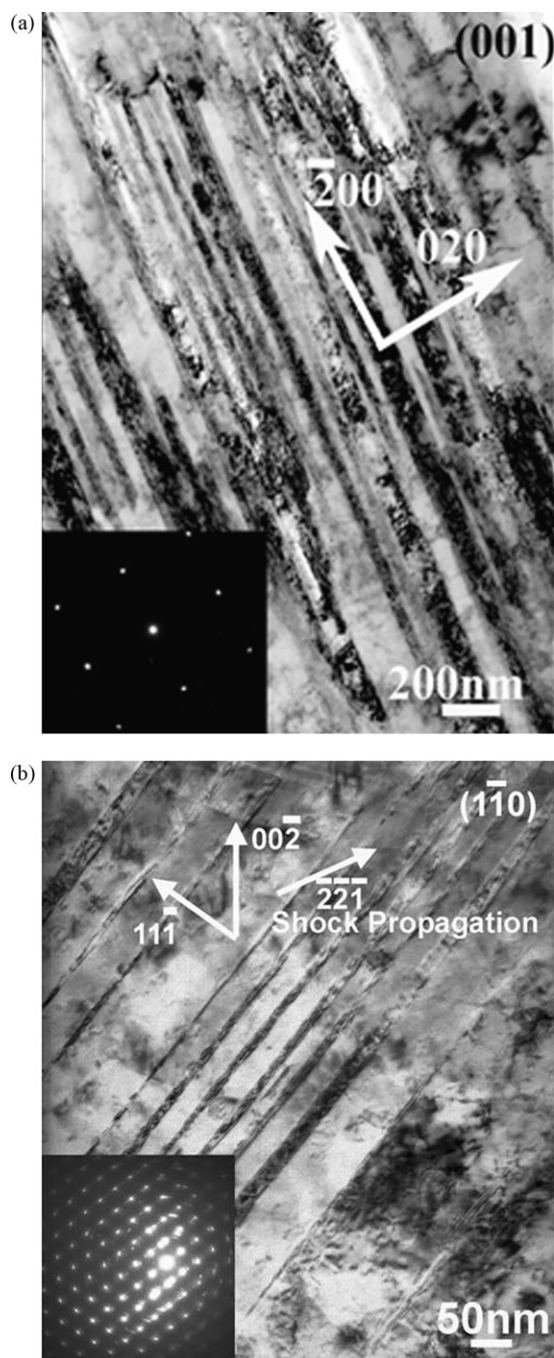
(a)

(b)

Fig. 5. (a) Microbands in 30 GPa post-shocked [2 2 1] copper; (b) bands on (1 1̄ 0) plane.

(a)

(b)

Fig. 6. (a) SEM for 57 GPa post-shocked copper samples; (b) "sub-bands" formed in the larger bands in B area for 57 GPa post-shocked [1 0 0] samples.

teristics. Murr and Staudhammer [34] measured the dislocation cell sizes in shock compressed Cu and Ni. For the pressure of 57 GPa, one would expect diameter around 90 nm. This value is consistent with Fig. 9(c). Cell-like structures with poorly defined cell walls are also observed in stainless steel [35]. If the shock pulse duration is low, the substructures are more irregular because there is insufficient time for the dislocations generated by the peak pressure (in the shock front) to equilibrate. Other studies [36,37] confirm substructure consisting of tangled dislocations in cellular arrays.

Fig. 8(a) shows the general view near the back surface of the specimen (foil parallel to shock front plane). A shear band with a width of about a 1.5 μm crosses the foil. Compared with the slip bands around it, this shear band is larger and breaks the other slip bands. The microbands in Fig. 8(a) have distinct characteristics. The vertical bands are larger than the horizontal ones; whereas the number of horizontal ones is much higher than that vertical ones. Fig. 8(b) is a detailed image of these slip bands. Two sets of slip bands having a width of about 0.5 μm are shown. The direction of vertical slip bands was identified as [1 1̄ 2], which might be the traces of (1̄ 1 1) plane. The horizontal bands seem to be cut by the vertical ones and recovery effects appear in these bands. By measuring the distances between the repeated structures in both Figs. 7(b) and 8(a), it was found that they have the same width of around 500 nm. The periodicity of the features of both the dislocations and bands is remarkable. It is speculated that these dislocation features are due to the recovered slip traces seen in Fig. 8(a).

Various microstructures on foils (1 0 0) perpendicular to the shock front were also observed, as shown in Fig. 9(a) and (b). Bands are the most prominent characteristics. Fig. 9(a) gives an overview of the bands in the entire sample. Recrystallization nuclei were observed within shear bands (indicated in this figure), which interact with these bands. In Fig. 8(b), bands are predominant in one orientation and interact with others in [1 1 0] ([2 2 0]) orientation, which indicates the traces of (1 1̄ 1) and/or (1̄ 1 1) planes.

co-workers [3,26,29,31] and Johari and Thomas [6] showed that twinning is a favored deformation mechanism under shock loading. Dislocation cell arrays can be seen in Fig. 7(b) and (c). Between these arrays, there are dislocation tangles and in some places the dislocation density is very high. The dislocation density was lower and the arrays were extended in the second thin foil along the shock direction (Fig. 7(c)). Mughrabi et al. [32] found some dislocation cell structures very similar to our observations, but they are quite unlike the cells observed by other investigators (e.g., Johari and Thomas [6]). Gray and Follansbee [33] concluded that increasing peak pressure or pulse duration decreased the observed dislocation cell size and increased the yield strength. The dislocation cells were extended and, therefore, showed some deformation charac-
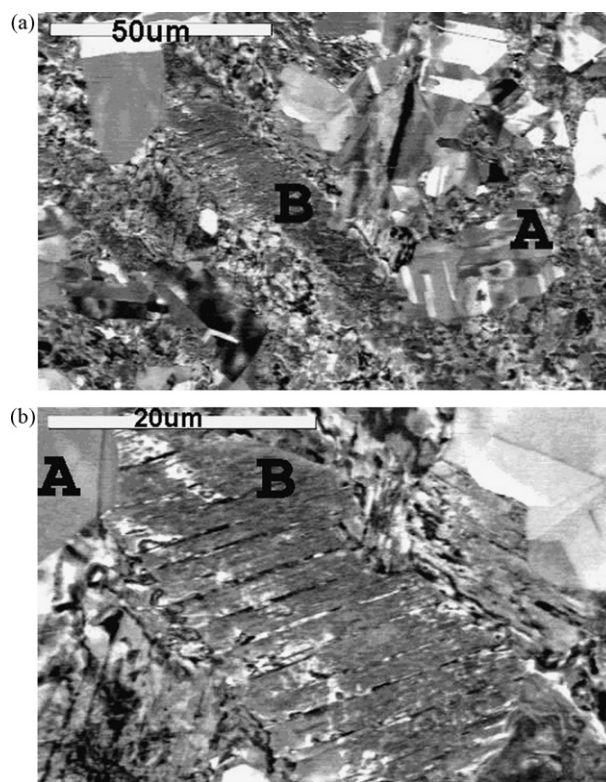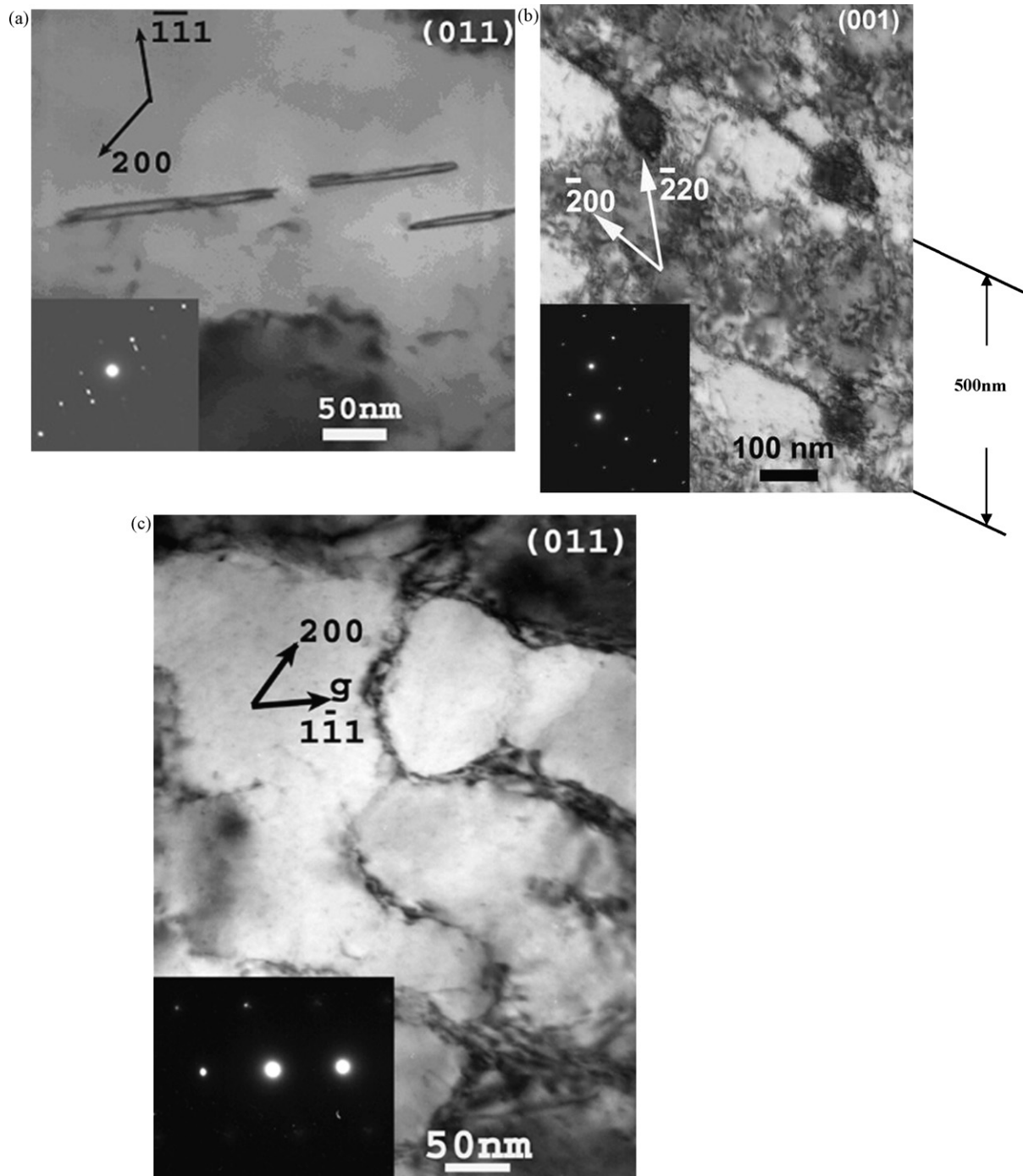
Fig. 7. (a) Micro-twins in 57 GPa post-shocked [0 0 1] copper with the habit plane of ($\bar{1}\,\bar{1}\,1$) shown at the electron beam direction of [0 1 1]; (b) dislocation structures showing periodicity; (c) the dislocation circles shown in the second thin foil along the shock direction.

3.4. [2 2 1] copper impacted at 57 GPa

The [2 2 1] copper samples shocked at 57 GPa were fully recrystallized. The SEM-ECC pictures show recrystallized grains and annealing twins (Fig. 10(a)). Fig. 10(b) shows the annealing twins and dislocations in proximity to the annealing twin boundaries.

This recrystallization is consistent with post-shock cooling calculations conducted by Cao et al. [38]. For 57 GPa, the calculated residual temperature is 420 K. Although this is sufficient for recrystallization at long times, the post-shock cooling effectively returns the temperature to 300 K in 20–40 s [38]. This would most probably not be sufficient for large-scale recrystallization. Cao et al. [38]

proposed that shear localization can lead to temperature rises of up to 500 K above the predictions for shock compression/isentropic release. Thus, it is the local shear localization, possible in monocrystals because of the absence of obstacle to slip that creates the localized regions of Fig. 6. This will be discussed further in Section 5.

4. Analysis of crystal plasticity

The four close packed planes and six close packed directions in fcc metals define 12 slip systems. Under conditions of uniaxial stress deformation, the critical resolved shear stress law in conjunction with Schmid factors can be used to predict the onset of plastic
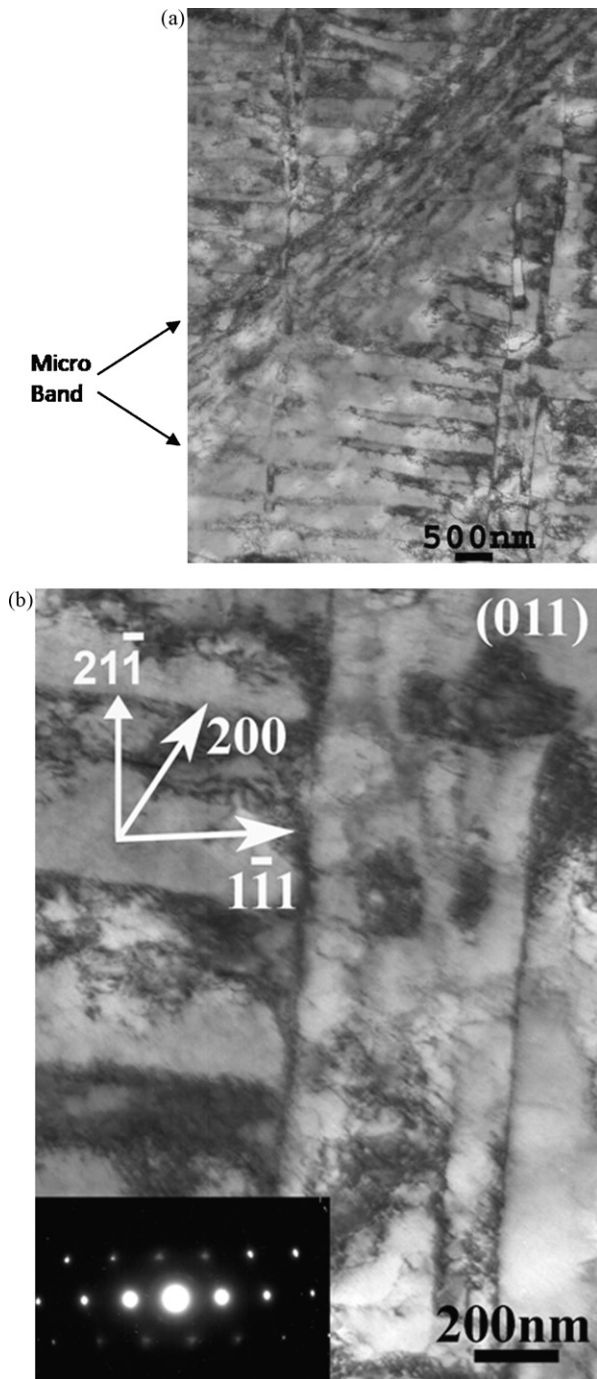
Fig. 8. (a) Micro shear band in 57 GPa impacted [0 0 1] copper (from Cao et al. [38], Fig. 6); (b) slip bands.

Fig. 9. (a) Microshear bands in 57 GPa impacted [1 0 0] copper; (b) broader band crossing narrower ones.

flow of the slip system with the highest resolved shear stress. These principles are the basis for crystal plasticity, and there have been many applications to non-uniaxial stress deformation, including shock loading of metals [39]. However, there has never been a study conducted to correlate expected slip system activity based on crystal plasticity with the residual microstructures of shock/recovered single crystals. The experiments performed in this work are ideally suited for this analysis.

For the shock loaded [0 0 1] and [2 2 1] crystals, we analyze the resolved shear stress for each of the {1 1 1}[0 1 1] slip systems using orthotropic elasticity assuming a homogeneous uniaxial strain compression. This is essentially an adaptation of the classic
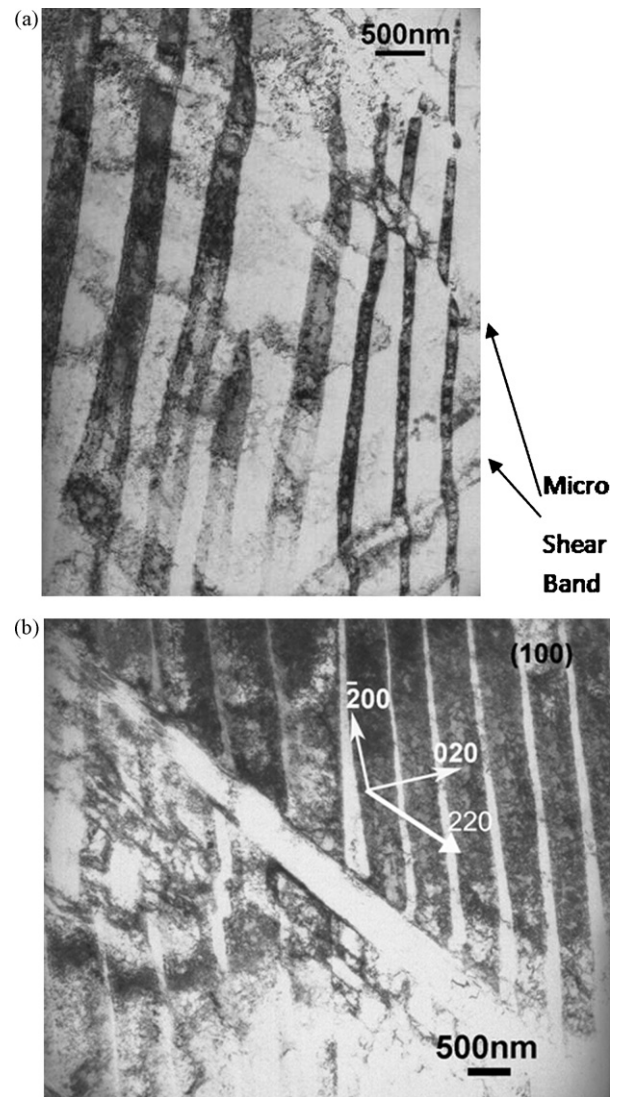
Schmid factors to the situation of shock loading. Second, using the same definitions for the slip planes and directions, we perform a kinematical analysis to determine what combinations of slip are consistent with uniaxial strain deformation. While there are many solutions, we find that only some are consistent with positive work on all of the slip system. The net magnitude of slip on each plane is then analyzed and comparisons to the observations of slip bands using SEM/SCC and TEM are made.

4.1. Analysis of the resolved shear stresses during the shock rise

For the purposes of this analysis, we have identified all of the slip systems in the [0 0 1] and [2 2 1] crystals relative to the shock propagation direction in Fig. 11. During a plate impact experiment the material is initially at zero strain and is subsequently subjected to a uniaxial elastic strain by the shock, hence the strain tensor is simply,

$$\begin{bmatrix} 0 & 0 & 0 \\ 0 & 0 & 0 \\ 0 & 0 & \varepsilon_{33} \end{bmatrix} \tag{1}$$

where ε_{33} is the elastic strain at the point of incipient plastic flow. The calculated values for 30 and 57 GPa are shown in Table 1. For
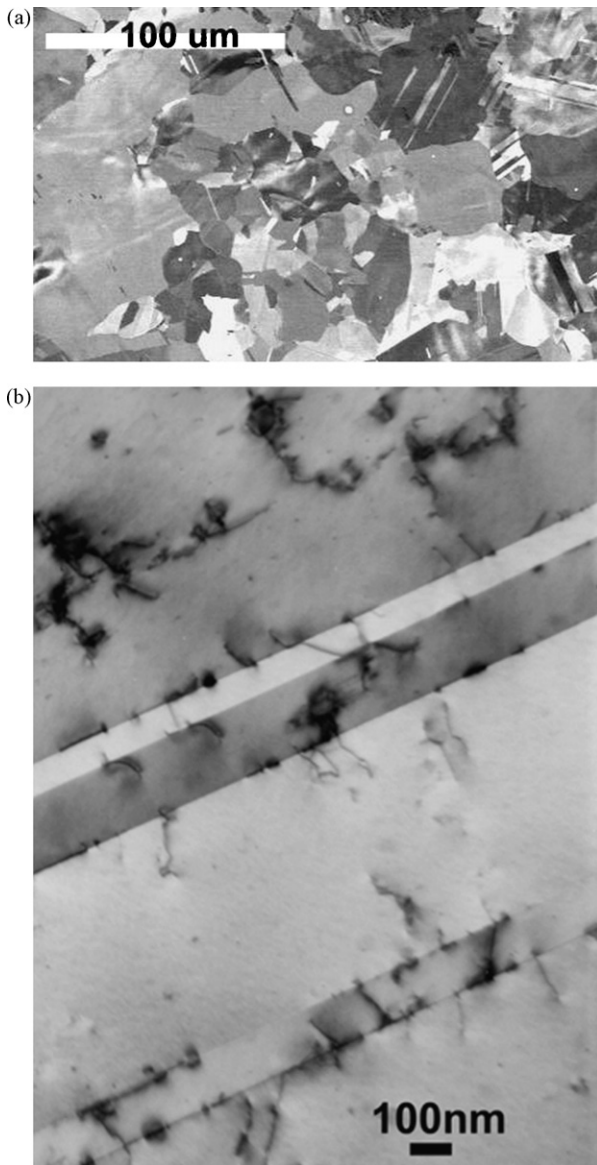
(a)

(b)

Fig. 10. (a) SEM-ECC showing recrystallized grains in 57 GPa shocked [2 2 1] sample; (b) TEM showing annealing twins as well as dislocations.

a given value of ε_{33}, the stress state is given by the following (e.g., [40], p. 132):

$$\sigma_{ij} = C_{ijkl}\varepsilon_{kl} \tag{2}$$

where C_{ijkl} is the elastic stiffness matrix with respect to the experimental coordinate system. The elastic stiffness matrix for copper in the crystallographic coordinate system ([1 0 0], [0 1 0], [0 0 1]) (e.g.,

Table 1
Uniaxial strains for shock loaded samples.

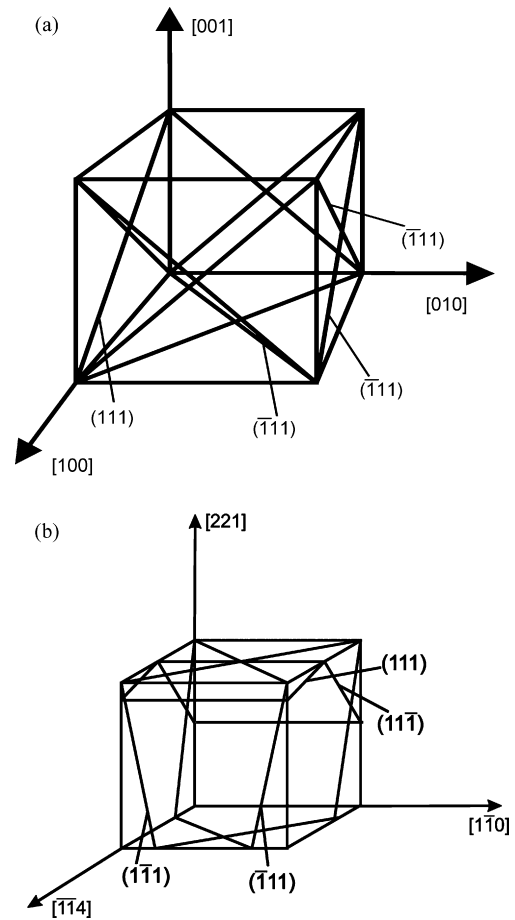| Pressure (GPa)	Volume (V)	V/V_0	$\varepsilon_{33} = \ln(V/V_0)$
30	9.56E-05	8.65E-01	−0.14527
57	8.85E-05	8.01E-01	−0.22201

(a)

(b)

Fig. 11. (a) Geometry of the slip systems in [1 0 0] monocrystal; (b) geometry of the slip systems in [2 2 1] monocrystal.

[41]) is:

$$[C_{ijkl}] = \begin{bmatrix} 168.4 & 121.4 & 121.4 & 0 & 0 & 0 \\ 121.4 & 168.4 & 121.4 & 0 & 0 & 0 \\ 121.4 & 121.4 & 168.4 & 0 & 0 & 0 \\ 0 & 0 & 0 & 75.4 & 0 & 0 \\ 0 & 0 & 0 & 0 & 75.4 & 0 \\ 0 & 0 & 0 & 0 & 0 & 75.4 \end{bmatrix} \tag{3}$$

For the [0 0 1] sample the experimental and crystallographic coordinate systems are the same and the calculated stresses expressed in terms of ε_{33} are listed in Table 2. As expected, there are only normal stresses acting on the unit cube due to the symmetry of the lattice structure with respect to the shock propagation.

For shock propagation along the [2 2 1] orientation, the elastic constants need to be rotated to a new coordinate system (with $[\bar{1}\,\bar{1}\,4]$, $[1\,\bar{1}\,0]$, $[2\,2\,1]$ axes), as shown in Fig. 1(c). The transformation

Table 2
Stresses with [0 0 1] shock compression direction, and with new coordinate system of $[\bar{1}\,\bar{1}\,4]$, $[1\,\bar{1}\,0]$, and $[2\,2\,1]$.

i, j	σ_{ij} (GPa)	
	[1 0 0]	[2 2 1]
11	$121\varepsilon_{33}$	$106.17\varepsilon_{33}$
12	0	0
13	0	$-6.95\varepsilon_{33}$
22	$121\varepsilon_{33}$	$75.28\varepsilon_{33}$
23	0	0
33	$168\varepsilon_{33}$	$230.2\varepsilon_{33}$

Table 3
Resolved shear stresses on the 12 slip systems with coordinates of [1 0 0], [0 1 0], and [0 0 1] for shocked [0 0 1] copper; right-hand column shows calculated shear strains for $P = 57$ GPa.

Slip systems number	Slip systems	Resolved shear stresses (GPa)	Shear strain γ^α
1	$(\bar{1}\,\bar{1}\,1)[\bar{1}\,1\,0]$	0	0
2	$(\bar{1}\,\bar{1}\,1)[1\,0\,1]$	$19.17\varepsilon_{33}$	0.2041
3	$(\bar{1}\,\bar{1}\,1)[0\,1\,1]$	$19.17\varepsilon_{33}$	0.2041
4	$(1\,1\,1)[\bar{1}\,1\,0]$	0	0
5	$(1\,1\,1)[\bar{1}\,0\,1]$	$19.17\varepsilon_{33}$	0.2041
6	$(1\,1\,1)[0\,\bar{1}\,1]$	$19.17\varepsilon_{33}$	0.2041
7	$(\bar{1}\,1\,1)[1\,1\,0]$	0	0
8	$(\bar{1}\,1\,1)[1\,0\,1]$	$19.17\varepsilon_{33}$	0.2041
9	$(\bar{1}\,1\,1)[0\,\bar{1}\,1]$	$19.17\varepsilon_{33}$	0.2041
10	$(1\,\bar{1}\,1)[1\,1\,0]$	0	0
11	$(1\,\bar{1}\,1)[\bar{1}\,0\,1]$	$19.17\varepsilon_{33}$	0.2041
12	$(1\,\bar{1}\,1)[0\,1\,1]$	$19.17\varepsilon_{33}$	0.2041

equation is (e.g., [40], p. 134):

$$C'_{ijkl} = l_{im}l_{jn}l_{ko}l_{lp}C_{mnop} \tag{4}$$

where the symbols l_{mn} are used to specify the cosines of the angles between the new coordinate system and the normal crystallographic axes. Performing this transformation the elastic constants with respect to the laboratory coordinate system is as follows in contracted form:

$$\begin{bmatrix} 203 & 115 & 106 & 0 & -27 & 0 \\ 115 & 219 & 75 & 0 & 16 & 0 \\ 106 & 75 & 230 & 0 & -7 & 0 \\ 0 & 0 & 0 & 75.4 & 0 & 16 \\ -27 & 16 & -7 & 0 & 60 & 0 \\ 0 & 0 & 0 & 16 & 0 & 83 \end{bmatrix} \tag{5}$$

Using Eq. (2) the stresses for the [2 2 1] sample with respect to the laboratory coordinate system were calculated in terms of ε_{33} and are listed in Table 4.

The resolved shear stresses on the 12 slip systems for the [0 0 1] and [2 2 1] samples can be calculated using the following equation,

$$\tau^\alpha = n^\alpha \times [\sigma]b^\alpha \tag{6}$$

where n^α is the unit vector normal to the slip plane in the laboratory coordinate system and b^α is the unit vector parallel to the direction of slip (which is co-linear with the Burgers vector) also in the laboratory coordinate system. Performing these calculation the resolved shear stress on the slip systems were calculated for the [0 0 1] and [2 2 1] samples and are given in the right-hand columns of Tables 3 and 4.

Table 4
Resolved shear stresses on the 12 slip systems in coordinate system $[\bar{1}\,\bar{1}\,4]$, $[1\,\bar{1}\,0]$, and $[2\,2\,1]$ for shocked $[2\,2\,1]$ copper; right-hand column shows calculated shear strains for $P = 57$ GPa.

Slip systems number	Slip systems	Resolved shear stresses (GPa)	Shear strain γ^α
1	$(1\,1\,\bar{1})[\bar{1}\,1\,0]$	0	0
2	$(1\,1\,\bar{1})[1\,0\,1]$	$52.5\varepsilon_{33}$	0.4763
3	$(1\,1\,\bar{1})[0\,1\,1]$	$52.5\varepsilon_{33}$	0.4763
4	$(\bar{1}\,\bar{1}\,\bar{1})[\bar{1}\,1\,0]$	0	0
5	$(\bar{1}\,\bar{1}\,\bar{1})[\bar{1}\,0\,1]$	$33.2\varepsilon_{33}$	0.2041
6	$(\bar{1}\,\bar{1}\,\bar{1})[0\,\bar{1}\,1]$	$33.2\varepsilon_{33}$	0.2041
7	$(\bar{1}\,1\,1)[1\,1\,0]$	$19.3\varepsilon_{33}$	0.2041
8	$(\bar{1}\,1\,1)[1\,0\,1]$	$25.8\varepsilon_{33}$	0.4082
9	$(\bar{1}\,1\,1)[0\,\bar{1}\,1]$	$6.5\varepsilon_{33}$	0
10	$(1\,\bar{1}\,1)[1\,1\,0]$	$19.3\varepsilon_{33}$	0.2041
11	$(1\,\bar{1}\,1)[\bar{1}\,0\,1]$	$6.5\varepsilon_{33}$	0
12	$(1\,\bar{1}\,1)[0\,1\,1]$	$25.8\varepsilon_{33}$	0.4082
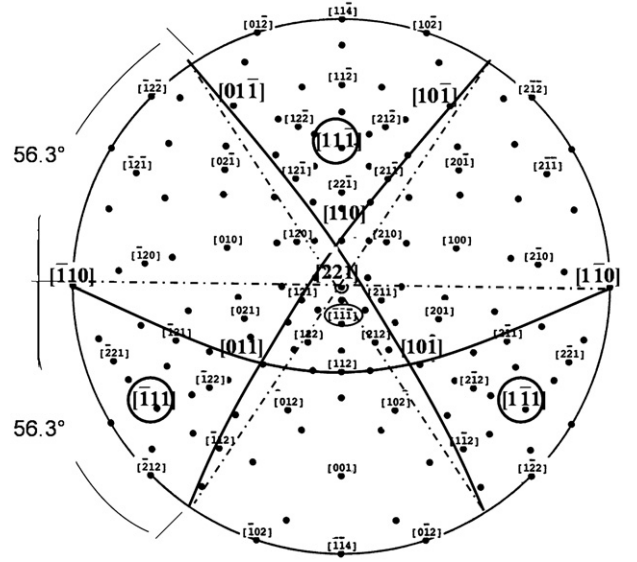
Fig. 12. [2 2 1] pole figure with $(11\bar{1})$, $(\bar{1}\bar{1}\bar{1})$, $(\bar{1}11)$ and $(1\bar{1}1)$ planes shown as solid lines.

4.2. Calculation of slip system activity

The calculated resolved shear stresses in the previous section are only an indication of the driving stress on the slip systems prior to plastic flow. In addition to driving stress, a compatibly condition needs to be met such that the sum of all slip system activity is consistent with the uniaxial strain condition. The deformation gradient matrix U can be written as follows for the shock imposed deformation

$$U = \begin{bmatrix} 0 & 0 & 0 \\ 0 & 0 & 0 \\ 0 & 0 & \dfrac{\partial u_z}{\partial z} \end{bmatrix} \tag{7}$$

The deviatoric component of the deformation gradient matrix u_D can be used to calculate the shear strains of eight independent slip systems and is,

$$u_D = u - u_v \tag{8}$$

where u_v is the volumetric component of the deformation gradient matrix and is given by the following equation,

$$u_v = \frac{1}{3}\frac{\partial u_z}{\partial z}[I] \tag{9}$$

where I is the identity matrix. Making the appropriate substitutions we have the following for the deviatoric component of the deformation gradient matrix as a function of the uniaxial strain imposed by the shock,

$$u_D = \frac{\partial u_z}{\partial z}\begin{bmatrix} -1/3 & 0 & 0 \\ 0 & -1/3 & 0 \\ 0 & 0 & -1/3 \end{bmatrix} \tag{10}$$

In this formulation we have made two assumptions: first that the compressibility of the Cu single crystal is isotropic; second, that the strength of the shocked material is negligible in comparison to the stress generated by the shock. This is certainly true in the case of our experiments where the shock pressures are on the order of 10's GPa whereas the Hugoniot elastic limit for single crystal Cu is estimated to be on the order of 0.01 GPa or less.

Our goal to determine the possible combinations slip system activity that are consistent with deviatoric component of the
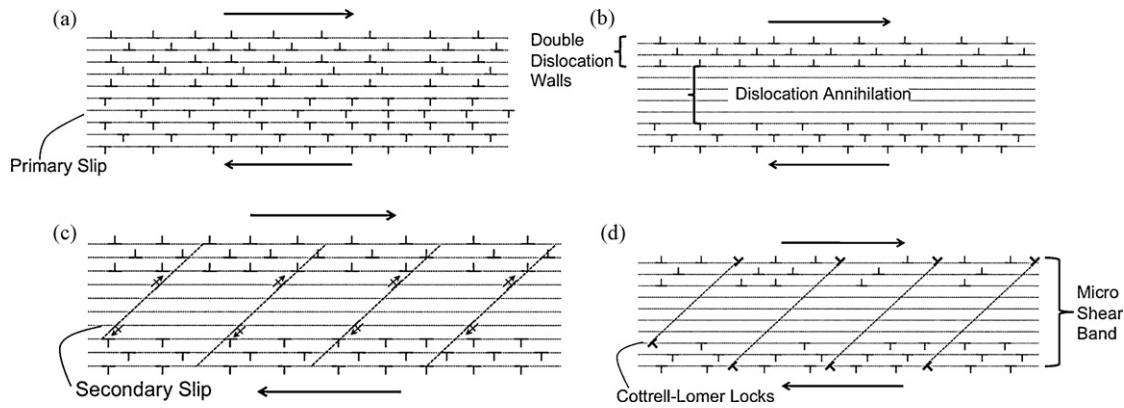
Fig. 13. Schematic representation of the formation of microbands (Huang-Gray [25] mechanism): (a) positive (top planes) and negative (bottom planes) dislocations forming on primary slip planes; (b) annihilation of dislocations in central planes leaving positive and negative double dislocation walls; (c) slip in secondary plane; (d) reaction of dislocations from primary and secondary planers forming Cottrell–Lomer locks.

displacement gradient matrix, which is given by the following equation ([42], p. 331).

$$u_D = \sum_{\alpha=1}^{n} \gamma^\alpha m_{ij}^\alpha \qquad (11)$$

where γ^α is the amount of slip that occurs for the slip system α, and n is the number of slip systems. m_{ij}^α is given by the following,

$$m_{ij}^\alpha = \frac{1}{2}(b_i^\alpha n_j^\alpha + b_j^\alpha n_i^\alpha) \qquad (12)$$

Florando et al. [43,44] have recently discussed this approach. Because we are working with the deviatoric component of the deformation gradient tensor only eight components are linearly independent. Therefore we can solve for the slip system activity of eight independent slip systems. For the fcc lattice, there are three slip directions on each of the four slip planes, and only two of the three slip directions on a given slip plane are independent. Consequently there are many solutions for sets of γ that satisfy Eq. (11). A computer program was written to solve for all of the possible sets of γ (792 in all). The solutions were then analyzed with respect to two criteria that make physical sense. The first is that shear on the slip system occurs in the same direction as the applied stress as calculated above. This leads to the following for the elastic work done at the point of incipient plastic flow,

$$W^\alpha = \int \gamma^\alpha d\tau \geq 0 \qquad (13)$$

The second criterion for selection of a physically plausible solution for slip is that the shear strains have the same symmetry as the crystal lattice with respect to the shock propagation. Employing these two criteria, lead to essentially only one solution of shear strains for both the [0 0 1] and [2 2 1] crystals as shown in the right-hand columns of Tables 3 and 4.

Due to symmetry of the sample with the [0 0 1] orientation with respect to the shock propagation, all four slip planes are equally active with two slip directions on each plane being equally active (eight slip systems equally active). In this situation, the primary, conjugate, and cross-slip planes are undefined. These shear strains were calculated for a pressure of 57 GPa.

In the case of the [2 2 1] crystal, we define the "primary slip plane" as the one that is most active and it is (1 1 $\bar{1}$). Therefore the conjugate slip plane is the ($\bar{1}$ $\bar{1}$ $\bar{1}$). There are two cross-slip planes that are equally active, those being the ($\bar{1}$ 1 1) and (1 $\bar{1}$ 1) planes. This is shown in Fig. 12. The net slip activity, which is the magnitude of the vector sum of the two slip directions on a given plane, was determined and we find the ratio of slip on the conjugate plane

relative to the primary is 0.61:1. Similarly the ratio of the slip on the cross-slip planes relative to the primary is 0.93:1. Therefore we would expect to see substantially more microstructural features associated with the primary plane, or perhaps the trace associated with the intersection of the primary and cross-slip or conjugate slip planes.

5. Microband formation and additional heating

The presence of profuse microbands in combination with dislocation cells corroborates the previous observations by Gray [23], Huang and Gray [24,25] and Sanchez et al. [26] in shock loaded FCC metals and alloys. The mechanism proposed by Huang and Gray [25] is presented in schematic form in Fig. 13. The monocrystalline nature of the specimens used in the current investigation is especially propitious for the formation of microbands because of the extended mean free path of dislocations. Thus, dislocations can travel unimpeded along the plane of maximum shear stress as shown in Fig. 13. In the case of edge dislocations, no cross-slip occurs dud to the nature of the burgers vector. The bottom part of Fig. 13(a) shows negative dislocations while the top part shows positive dislocations traveling in the opposite sense. Huang and Gray [25] proposed that in the regions where these dislocations are adjacent, they annihilate each other, creating dislocation-free channels surrounded by double dislocation wall arrangements (Fig. 13(b)). Slip on secondary systems (Fig. 13c) interacts with primary slip and leads to the formation of Cottrell–Lomer locks, blocking the slip (Fig. 13d). These microbands were also observed by Sanchez et al. [25] in shock loaded copper. They present a similar mechanism for their formation. Although Gray et al. [5] states that the incidence of these bands increases with the residual (post-shock) strain, in our single crystals the profuse microband formation can be envisaged to occur without significant residual strain, especially since a great care was taken to ensure a uniaxial strain state by momentum traps. Fig. 14 shows parallel microbands that alternating senses of shear. Thus, although local portions of the crystal are translated, the overall (global) strain is zero in the schematic. The localized
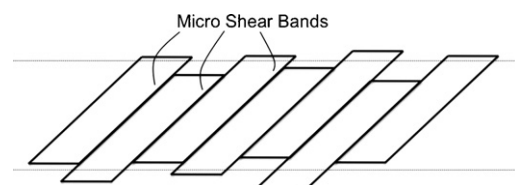

Fig. 14. Multiple microshear band formation with alternating senses leading to self compensating situation and resulting in zero net residual strain.
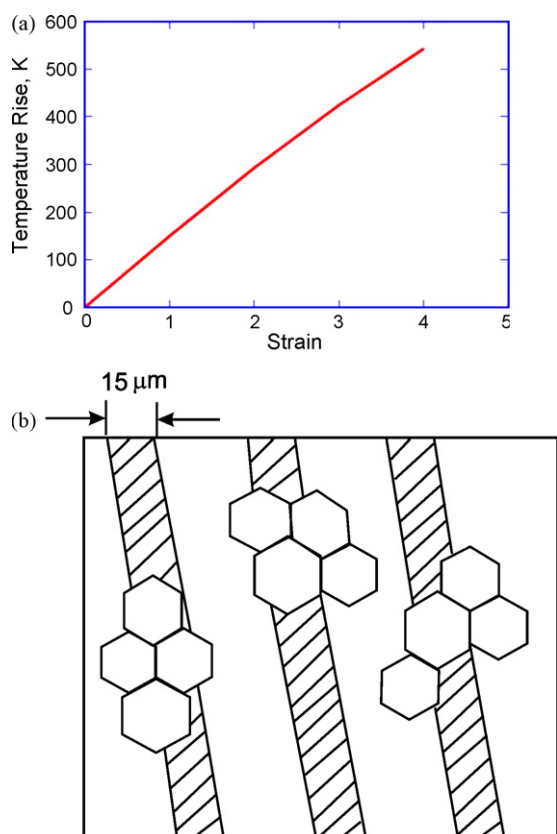
Fig. 15. (a) Temperature rise due to plastic deformation (from Cao et al. [38], Fig. 15); (b) schematic illustration of nucleation of recrystallized grains at microshear bands.

shear by the microbands can lead to enhanced heat generation and is, indeed, a redundant plastic deformation process.

The temperature increase produced by plastic deformation has been expressed by Cao et al. [38] as:

$$T^* = 1 - \exp\left[\frac{-0.9\left(1 + C\log \dot{\varepsilon}/\dot{\varepsilon}_0\right)}{\rho C_p (T_m - T_r)} x \left(\sigma_0\varepsilon + \frac{B\varepsilon^{n+1}}{n+1}\right)\right]$$

where $T_r = 90$ K, $T_m = 1356$ K, $B = 53.7$ MPa, $C = 0.026$, $\sigma_0 = 330$ PPa (the strength of shock hardened copper), $n = 0.56$, $m = 1.04$, $\rho = 9.05$ g/cm^3, $C_p = 260$ J/kg K. Fig. 15(a) shows the increase in temperature as a function of shear strain. Thus, a concentrated shear inside a microband can generate significant temperature increases.

Thus, one can envisage the nucleation of recrystallization nuclei at microbands, where the temperature can reach values sufficient for recrystallization. Lassila et al. [22] discussed the residual temperatures in shock compressed polycrystals and also arrived at the conclusion that additional heating is required. The residual temperatures are:

$P = 30$ GPa : 260 K
$P = 57$ GPA : $T = 508$ K

The cooling rate can be estimated from the calculations by Cao et al. [38] who obtained the following time for cooling to 300 K:

$P = 57$ GPa : $t = 20$ s

For the lower pressure, the temperature does not even reach the room temperature value. It is instructive to compare these times with the times for static recrystallization reported in the literature [45]. Paul et al. [46] report initiation of recrystallization after 60 s anneal at 773 K. Xiao et al. [47] report recrystallization of fatigue

bands after electropulsing to a temperature rise (T) of 457 K. Huh et al. [48] observe recrystallization in copper after a 673 K anneal for 1 h.

Thus, it is highly unlikely that the residual temperature after shock compression to $P = 57$ GPa (which is only 508 K) is sufficient for recrystallization. However, the additional heavy generation of deformation at the microbands can increase the local temperature to the level where recrystallization nuclei can be formed. This is shown in a schematic fashion in Fig. 15(b). Recrystallized grains are initiated at the microbands. The picture is similar to the one proposed by Xiao et al. [47]. Andrade et al. [18] subjected shock hardened copper to plastic deformation at elevated temperatures and did not observe Recrystallization at 473 K. However, at 573, and 673 K, recrystallization occurred in the deformation regions. This process initiated at 523 K.

6. Summary and conclusions

Monocrystalline copper samples with orientations [0 0 1] and [2 2 1] were subjected to shock/recovery experiments at 30 and 57 GPa from an initial temperature of 90 K. The microstructure evolution and slip system activity were investigated. The principal results are:

- The different crystalline orientations (in our case [0 0 1] and [2 2 1], respectively), exhibited different post-shocked microstructures because of differences in resolved shear stresses on the slip systems;
- For the [2 2 1] system, the highest resolved shear stress on the most solicited system is equal to $52.5\varepsilon_{33}$, while for [0 0 1] it is equal to $19.17\varepsilon_{33}$. It is suggested that the higher resolved stress, in combination with the lower number of systems activated for [2 2 1] leads to greater localization with a higher local temperature rise. Whereas the post-shock uniform temperature reaches 420 K and cools to 300 K in 20–40 s, the local temperature rise in a shear localization region can reach much higher values. It is proposed that this leads to a more prevailed recrystallization for [2 2 1] at 57 GPa.
- For the [0 0 1] specimen impacted at 30 GPa, SEM-ECC pictures show the traces of slip bands on the surface of the sample. Large deformation bands (microbands) and stacking faults were revealed by TEM.
- The [2 2 1] specimen impacted at 30 GPa shows traces of slip on the surface. Both deformation bands and slip bands were observed.
- For the [0 0 1] specimen impacted at higher pressure of 57 GPa, there are some bands and isolated recrystallized regions. Different defects, such as bands, dislocations and microtwins are revealed. These defect structures are distributed randomly through the entire specimen.
- The formation of microbands is interpreted in terms of the Huang and Gray [25] mechanism. This mechanism proposes that double dislocation walls are formed and subsequently blocked by slip on secondary slip systems, the reactions producing Cottrell–Lomer locks.
- The [2 2 1] specimens impacted at 57 GPa were fully recrystallized. Annealing twins were found inside these grains, a characteristic feature of static recrystallization.

References

[1] G.T. Gray III, in: M.A. Meyers, L.E. Murr, K.P. Staudhammer (Eds.), Shock-Waves and High-Strain-Rate Phenomena in Materials, Marcel Dekker, NY, 1992, pp. 899–911.
[2] L.E. Murr, Scripta Materialia 12 (1978) 201–206.
[3] L.E. Murr, in: M.A. Meyers, L.E. Murr (Eds.), Shock Waves and High-Strain-Rate Phenomena in Metals, Plenum, NY, 1981, pp. 607–673.
[4] F.I. Grace, Journal of Applied Physics 40 (1969) 2649–2653.
[5] G.T. Gray III, P.S. Follansbee, C.E. Frantz, Materials Science and Engineering A 111A (1989) 9–16.
[6] O. Johari, G. Thomas, Acta Metallurgica 12 (1964) 1153–1159.
[7] R.L. Nolder, G. Thomas, Acta Metallurgica 11 (1963) 994–995.
[8] R.L. Nolder, G. Thomas, Acta Metallurgica 12 (1964) 227–240.
[9] R.J. De Angelis, J.B. Cohen, Journal of Metals 15 (1963) 681–690.
[10] P.S. Follansbee, in: L.E. Murr, K.P. Staudhammer, M.A. Meyers (Eds.), Metallurgical Applications of Shock-Wave and High-Strain-Rate Phenomena, Marcel Dekker, New York, 1986, pp. 451–479.
[11] P.E. Senseny, J. Duffy, H. Hawley, Journal of Applied Mechanics 45 (1978) 60–66.
[12] T. Glenn, W. Bradley, Metallurgical Transactions 4 (1973) 2343–2348.
[13] J.R. Klepaczko, Materials Science and Engineering 18 (1975) 121–135.
[14] P.S. Follansbee, G.T. Gray III, Materials Science and Engineering A 138A (1991) 23–31.
[15] U.F. Kocks, Journal of Engineering Materials and Technology 98 (1976) 76–85.
[16] H. Mecking, U.F. Kocks, Acta Metallurgica 29 (1981) 1865–1875.
[17] P.S. Follansbee, U.F. Kocks, Acta Metallurgica 36 (1988) 81–93.
[18] U.R. Andrade, M.A. Meyers, K.S. Vecchio, A.H. Chokshi, Acta Metallurgica 42 (1994) 3183–3195.
[19] M.A. Meyers, U.R. Andrade, A.H. Chokshi, Metallurgical and Materials Transactions 26A (1995) 2881–2893.
[20] U.R. Andrade, M.A. Meyers, A.H. Chokshi, Scripta Metallurgica et Materialia 30 (1994) 933–938.
[21] W.H. Gourdin, D.H. Lassila, Materials Science and Engineering A 151A (1992) 11–18.
[22] D.H. Lassila, T. Shen, B. Cao, M.A. Meyers, Metallurgical and Materials Transactions A 35A (2004) 2729–2739.
[23] G.T. Gray III, Acta Metallurgica 36 (1988) 1745–1754.
[24] J.C. Huang, G.T. Gray III, Metallurgical and Material Transactions A 20A (1989) 1061–1075.
[25] J.C. Huang, G.T. Gray III, Acta Metallurgica 37 (1989) 3335–3347.
[26] J.C. Sanchez, L.E. Murr, K.P. Staudhammer, Acta Materialia 45 (1997) 3223–3235.
[27] P. Wagner, O. Engler, K. Lücke, Acta Materialia 43 (1995) 3799–3812.
[28] R. Zauter, F. Petry, M. Bayerlein, C. Sommer, H.J. Christ, H. Mughrabi, Philosophical Magazine A 66A (1992) 425–436.
[29] B. Gonzalez, L.E. Murr, O.L. Valerio, E.V. Esquivel, H. Lopez, Materials Characterization Journal 49 (2002) 359–366.
[30] M.A. Meyers, F. Gregori, B.K. Kad, M.S. Schneider, D.H. Kalantar, B.A. Remington, G. Ravichandran, T. Boehly, J.S. Wark, Acta Materialia 51 (2003) 1211–1228.
[31] F. Greulich, L.E. Murr, Materials Science and Engineering 39 (1979) 81–93.
[32] H. Mughrabi, T. Ungar, W. Kienle, M. Wilkens, Philosophical Magazine A 53A (1986) 793–813.
[33] G.T. Gray III, P.S. Follansbee, in: C.Y. Chiem, H.D. Kunze, L.W. Meyers (Eds.), Impact Loading and Dynamic Behavior of Materials, Informationsgesellschaft, Verlag, 1988, pp. 541–548.
[34] L.E. Murr, K.P. Staudhammer, Materials Science and Engineering 20 (1975) 35–46.
[35] M.A. Meyers, Dynamic Behavior of Materials, John Wiley and Sons, Inc., New York, 1994, pp. 382–447.
[36] L.F. Trueb, Journal of Applied Physics 40 (1969) 2976–2987.
[37] L.E. Murr, H.R. Vydyanath, J.V. Foltz, Metallurgical Transactions 1 (1970) 3215–3233.
[38] B.Y. Cao, D.H. Lassila, M.S. Schneider, B.K. Kad, C.X. Huang, Y.B. Xu, D.H. Kalantar, B.A. Remington, M.A. Meyers, Materials Science and Engineering A 409 (2005) 270–281.
[39] R. Becker, International Journal of Plasticity 20 (2004) 1983–2006.
[40] J.F. Nye, Physical Properties of Crystals, Oxford University Press, London, 1969.
[41] M.A. Meyers, K.K. Chawla, Mechanical Behavior of Materials, Prentice-Hall, Inc., Upper Saddle River, NJ, 2002.
[42] U.F. Kocks, C.N. Tomé, H.R. Wenk, Texture and Anisotropy, Cambridge University Press, 1998.
[43] J.N. Florando, M. Rhee, A. Arsenlis, M.M. LeBlanc, D.H. Lassila, Philosophical Magazine Letters 86 (2006) 795–805.
[44] J.N. Florando, M.M. LeBlanc, D.H. Lassila, Scripta Materialia 57 (2007) 537–540.
[45] F.J. Humphreys, M. Hatherly, Recrystallization and Related Annealing Phenomena, Pergamon Press, 1996.
[46] H. Paul, J.H. Drian, Z. Jasienski, Acta Materialia 50 (2002) 815–830.
[47] S.H. Xiao, J.D. Guo, S.D. Wu, G.H. He, S.X. Li, Scripta Materialia 46 (2002) 1–6.
[48] M.Y. Huh, Y.S. Cho, O. Engler, Materials Science Engineering A 247A (1998) 152–164.